Ion bipolar junction transistors

Klas Tybrandt[a], Karin C. Larsson[b], Agneta Richter-Dahlfors[b], and Magnus Berggren[a,1]

[a]Linköping University, Department of Science and Technology, Organic Electronics, SE-601 74 Norrköping, Sweden; and [b]Department of Neuroscience, Karolinska Institutet, SE-171 77 Stockholm, Sweden

Edited by Howard Reiss, University of California, Los Angeles, CA, and approved April 15, 2010 (received for review December 2, 2009)

Dynamic control of chemical microenvironments is essential for continued development in numerous fields of life sciences. Such control could be achieved with active chemical circuits for delivery of ions and biomolecules. As the basis for such circuitry, we report a solid-state ion bipolar junction transistor (IBJT) based on conducting polymers and thin films of anion- and cation-selective membranes. The IBJT is the ionic analogue to the conventional semiconductor BJT and is manufactured using standard microfabrication techniques. Transistor characteristics along with a model describing the principle of operation, in which an anionic base current amplifies a cationic collector current, are presented. By employing the IBJT as a bioelectronic circuit element for delivery of the neurotransmitter acetylcholine, its efficacy in modulating neuronal cell signaling is demonstrated.

ionic transistor | ionic transport | conducting polymers | cell signaling

Numerous biochemical, biomedical and clinical applications demand technology allowing for the spatiotemporally controlled delivery of ions and biomolecules. In order to gain dynamic control of cellular microenvironments, substance delivery in complex high-resolution patterns where each point of delivery is individually addressable is required. In analogy to the addressing schemes found in active matrix displays (1, 2), addressability in active chemical circuits can be achieved by introducing transistor functionality into each delivery point. Transistors are generally three-terminal devices in which the current between the first and second terminals is controlled by an electric signal applied to the third. The semiconductor solid-state transistor (3) is the key component that enables amplification, addressing, and processing of electronic signals in circuits. Analogously, a transistor based on transport of ions rather than electrons would render the same functionality possible in chemical circuits, e.g., for addressable delivery of charged ions and biomolecules. To date, few reports of transistor-like active control of ion transport have been published (4–8). The principle of operation in the majority of these devices is the modulation of the surface charge in nanochannels and nanoporous membranes. However, these devices are typically difficult to manufacture, hard to integrate into circuits, and do not operate well at the high ion concentrations required to generate physiologically relevant conditions.

Bipolar junction transistors (BJTs) (3) are a major class of transistors with their own nomenclature: The input, output, and control terminals are denoted emitter, collector, and base, respectively. A *pnp*-BJT can bee seen as two *pn*-junctions sharing a narrow base region, where the emitter and collector are *p*-doped and the base is *n*-doped. Anion- and cation-selective membranes (9) are the ionic equivalents to *n*- and *p*-doped semiconductors, respectively. These membranes contain fixed ionic groups compensated by mobile ions of the opposite charge (counterions). Mobile ions of the same charge (coions) are electrostatically repelled when the concentration of the surrounding electrolyte is well below that of the fixed charges (Donnan exclusion) (9). A bipolar membrane (BM) is a sandwich of an anion- and a cation-selective membrane (10). BMs exhibit several similarities to bipolar semiconductor *pn*-junction diodes, such as current rectification. The introduction of a neutral intermediate membrane layer, separating the two charged membranes, maintains a high current rectification ratio (10, 11). A BM separating two electrolytes is biased in the forward direction when a positive voltage is applied to the electrolyte contacting the cation-selective side (Fig. 1*A*). This causes accumulation of mobile ions in between the two charged membranes, resulting in a high ionic current through the BM. In reverse bias, the region in between the membranes is depleted of mobile ions, and the ionic current is significantly lower (11).

Inspired by the similarities of *pn*-junctions and BMs, we have developed a solid-state ion bipolar junction transistor (IBJT). Its use as a circuit element for neurotransmitter delivery was demonstrated by its dynamic control of the physiological microenvironment of neuronal cells via acetylcholine (ACh) delivery. Based on the theory of ion transport through selective membranes, a model of operation is proposed and compared with the characterization.

Results and Discussion

Materials and Device Architecture. The IBJT consists of two BMs, emitter-base and collector-base, with the same base region sharing a neutral intermediate layer (Fig. 1 *B* and *C*). The emitter and collector regions are both cation-selective while the base region is anion-selective. Thus, the configuration is equivalent to the electronic *pnp*-BJT. The IBJT device is fabricated from a thin film of the conductive polymer (12, 13) poly(3,4-ethylenedioxythiophene) (14) doped with the polyanion poly(styrenesulfonate) (PEDOT:PSS) coated on a plastic (PET) foil. Patterned PEDOT:PSS electrodes (15) together with aqueous electrolytes serve as the ion supply terminals according to the electrochemical reaction $\mathrm{PEDOT^+{:}PSS^-} + \mathrm{M^+(aq)} + \mathrm{e^-} \Leftrightarrow \mathrm{PEDOT^0} + \mathrm{M^+{:}PSS^-}$. The cation-selective emitter and collector regions comprise overoxidized (16) PEDOT:PSS. An insulating SU-8 film is deposited on top of the PEDOT:PSS pattern with openings located at the electrodes and at the junction (Fig. 1*D*). The emitter and collector are then connected by a junction consisting of a neutral cross-linked poly(ethylene glycol) (PEG) gel layer (Fig. 1 *C* and *D*). An anion-selective membrane, Fumatech FAB, is applied over the PEG gel, defining the base. Finally, the stack is sealed by a polydimethylsiloxane (PDMS) layer.

Modes of Operation and Transport Equations. Throughout this work the common-emitter transistor configuration is used (Fig. 1*B*). When operated in the cutoff mode, both the emitter-base (E-B) and the collector-base (C-B) diodes are reversely biased. The ion concentration in the bulk of the junction (c_J) is then low, and consequently the current between the emitter and collector (I_C) is small. After reversing the bias voltage of only the E-B diode, the transistor operates in active mode. As c_J increases, both I_C and the resistive potential drop along the emitter (ΔV_E) rise. This causes the potential drop across the E-B junction

Author contributions: K.T., K.C.L., A.R.-D., and M.B. designed research; K.T. and K.C.L. performed research; K.T. and K.C.L. analyzed data; and K.T., K.C.L., A.R.-D., and M.B. wrote the paper.

The authors declare no conflict of interest.

This article is a PNAS Direct Submission.

[1]To whom correspondence should be addressed. E-mail: magbe@itn.liu.se.

This article contains supporting information online at www.pnas.org/lookup/suppl/doi:10.1073/pnas.0913911107/-/DCSupplemental.

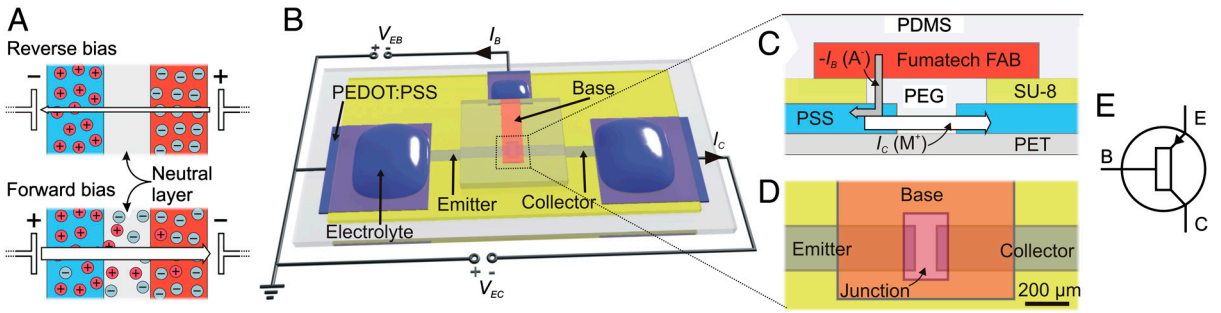

Fig. 1. Architecture of the IBJT. (*A*) The principal device structure of a BM, including a neutral intermediate membrane layer. In reverse and forward bias voltage, mobile ions are extracted from or accumulate within the intermediate layer, respectively. This results in ionic current rectification. (*B*) The IBJT biased according to the common-emitter configuration. PEDOT:PSS electrodes with aqueous electrolytes generate the ionic currents within the device. Emitter and collector (cation selective, L × W = 1.5 × 0.2 mm) meet the base (anion selective) defining the junction. (*C*) Vertical cross section along the emitter-collector configuration (not to scale). The emitter and collector (~250 nm thick PSS) are patterned on top of a PET substrate. A crosslinked PEG gel (referred to as the junction) is employed into the opening of the 10 μm thick SU-8 insulating layer. The base (~20 μm thick) contacts the gel and is covered by a PDMS seal layer. I_C is the flow of cations (M^+) from the emitter to the collector while I_B, in steady state, primarily consists of anions (A^-) migrating from the base to the emitter. (*D*) Top-down view of the IBJT. Emitter and collector are horizontally separated by 100 μm and the base covers the whole junction area. (*E*) The proposed circuit symbol of the *pnp*-IBJT.

to decrease until the base current (I_B) equals the E-B leakage current (steady state). Because ΔV_E is resistive and equals the emitter-base voltage (V_{EB}) in magnitude, the emitter current (I_E) and thus I_C are expected to depend linearly on V_{EB}: $I_C = R_E \cdot (V_{EB} - V_T)$ where V_T is the threshold voltage.

Charge transport equations for BJTs are commonly expressed assuming a 1D model, and a similar approach is employed here. By assuming that V_{EB} only modulates c_J and that c_J only varies along the direction from emitter to collector, the model system can be simplified to the E-J-C stack. This stack can be modeled using the transport theory developed for electrolyte-cation selective membranes (17) (*SI Text*). A linear diffusion gradient is created from emitter to collector in the bulk of the junction (Fig. 2), and the resulting I_C is proportional to ∇c_J. At the J-C interface a space charge region is formed with a low c_J and a high electric field (18, 19). In the cutoff mode the overall c_J is low and the entire potential drop occurs across the junction. Conversely, in the active mode c_J is high and the potential drop is more evenly distributed along E-J-C. When V_{EB} approaches $V_{EC}/2$, the transistor operation turns into the so-called saturation mode. At this mode of operation ion accumulation occurs in the junction region, resulting in a failure of membrane selectivity causing a high I_B value.

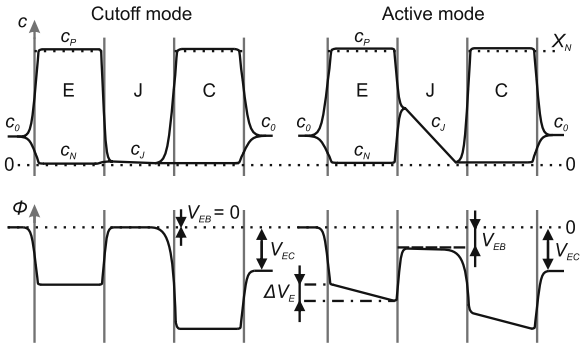

Fig. 2. Schematic drawing of ion concentrations and electric potentials along emitter-collector in the active- and in the cutoff mode. The salt concentration of the electrolytes (c_0) is lower than the concentration of negative fixed charges in the membranes (X_N). In the emitter and the collector, the concentration of mobile cations (c_P) is high while the concentration of mobile anions (c_N) is low. In the cutoff mode, the salt concentration in the junction (c_J) is low and therefore the potential (Φ) drop primarily occurs across this region. In the active mode, c_J is higher and the potential drop is split over the emitter (ΔV_E), the collector and the junction.

IBJT Characterization. Aqueous 0.1 M NaCl electrolytes were employed to all electrode configurations and the transfer curve was obtained by measuring I_C, keeping $V_{EC} = 10$ V and scanning V_{EB} back and forth between −0.5 to 4.5 V at a 2.5 mV/s scan rate (Fig. 3*A*). The onset threshold of I_C occurs at $V_T = 0.7$ V after which I_C increases linearly versus V_{EB}, as predicted. Interestingly, at this scan rate only minor hysteresis was present. The I_B leakage, primarily due to anions that escape through the emitter, increases as c_J becomes higher. Further, the current-voltage output characteristics were obtained by ramping V_{EC} for different fixed values of V_{EB} (Fig. 3*B*). By keeping $V_{EC}/2 > V_{EB}$ the transistor is operated in the active mode. As predicted, I_C is constant with respect to V_{EC} and is entirely modulated by V_{EB}. At $V_{EC} = 10$ V, the I_C on-off ratio between $V_{EB} = 4$ V and 0 V is 100. The gain at $V_{EB} = 4$ V is: $g = I_C/I_B = 10$.

The amount of anionic charge in the junction (Q_J) is expected to depend linearly on I_C, which was found to depend linearly on V_{EB} (see Fig. 3*A*). To verify this, the IBJT was first operated at $V_{EC} = 10$ V for different fixed V_{EB} values at steady state. V_{EC} and V_{EB} were then switched to 0 V and −2 V, respectively, at the same time as I_B was recorded in order to estimate Q_J. We found a linear relationship between Q_J and V_{EB} (Fig. 3*C*). Q_J at $V_{EB} = 4$ V corresponds to a concentration of 0.6 M NaCl at the emitter, a reasonable concentration for functional selective membranes (9). The on-off switching transients were measured by applying voltage steps to V_{EB} keeping $V_{EC} = 10$ V (Fig. 3*D*). When switched on, I_C rises quickly after an initial delay and reaches steady state. When V_{EB} is turned off the ions leave the junction, followed by a fast decrease in I_C as the junction becomes depleted. The 90% rise time of I_C is 12 s and the 10% fall time is 5 s (see Fig. 3*D*). The E-B diode was characterized separately by disconnecting V_{EC} and scanning V_{EB} from −5 V to 5 V (5 mV/s) (Fig. 3*E*). We measure a current rectification ratio ($|I_B(5\text{ V})/I_B(-5\text{ V})|$) of 39; which compares well with previously reported rectification characteristics of BMs (20). No pronounced field-enhanced dissociation of water was observed, as I_B remains low at reverse bias for the voltage region studied here.

In the characterization above, the IBJT shows good performance at high salt concentrations, thus enabling biological applications at physiological conditions. The functionality of the IBJT lies in the ion selectivity of the materials, which is less sensitive to high salt concentration than the surface effects utilized in nanofluidic transistors and diodes (5–8, 21). The use of bulk material properties rather than surface effects allows for devices with features in tens and hundreds of micrometers, enabling standard parallel microfabrication. However, it is likely that the performance of the IBJT can benefit from miniaturization, e.g., the

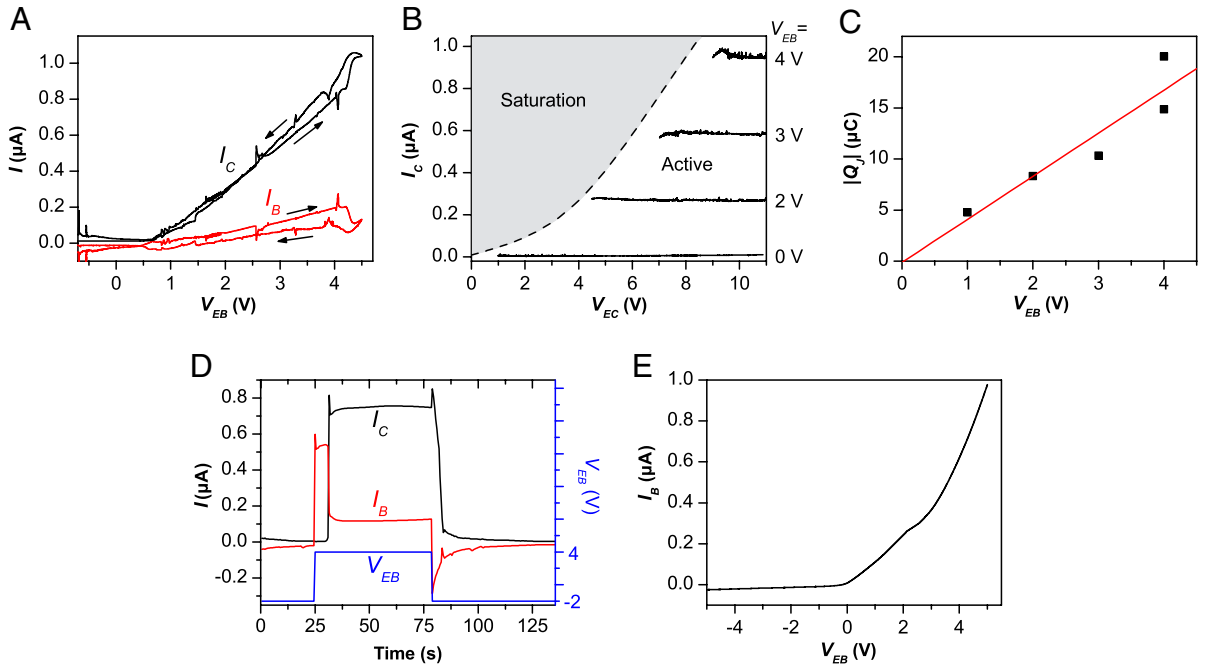

Fig. 3. Characteristics of the IBJT. (*A*) The transfer curve reveals a linear relationship between I_C and V_{EB}, with only minor hysteresis. I_B is higher in the forward scan due to injection of ions into the junction. (*B*) The output characteristics of the IBJT shows ion current saturation in the active mode. The saturation mode (gray region) is avoided in these scans. (*C*) The amount of anionic charge in the junction (Q_j) versus different V_{EB}. A linear fit to the data is displayed in red. (*D*) The switching transient for a voltage step in V_{EB}. The rise and fall of I_C correlates with positive and negative I_B, respectively. (*E*) Current versus voltage characteristics for the emitter-base diode circuit (V_{EC} disconnected). The expected rectification of the ionic current is observed.

switching speed is expected to increase. Polymers can readily be patterned on the nanoscale (22), provided that the material has a continuous phase. Whether the IBJT is functional at these dimensions is at this point unclear.

The IBJT as the Active Control Element of ACh Delivery. We recently demonstrated the use of organic conducting materials as a communication interface for translating electronic signals into precise delivery of chemical messengers, such as ions (e.g., Na^+, K^+, Ca^{2+}) and neurotransmitters (e.g., ACh) (23–25). In order to generate complex, high-resolution signaling patterns typical of neuronal cell signaling, matrix-addressed delivery systems are required. This could be accomplished if ion transistors actively controlled the release from each delivery point. To test if the IBJT could be used as an addressable delivery point for modulation of neuronal signaling, aqueous ACh solution was placed on the emitter electrode, whereas human neuroblastoma SH-SY5Y cells were cultured on the collector electrode (Fig. 4*A*). As SH-SY5Y cells express receptors for ACh, they rapidly respond to ACh stimulation by opening of membrane bound ion channels that promotes Ca^{2+} influx (26). Changes in the intracellular Ca^{2+} concentration, $[Ca^{2+}]_i$, can be monitored in real-time by fluorescence microscopy. Keeping the IBJT in the off-state ($V_{EC} = 10$ V and $V_{EB} = -1$ V), $[Ca^{2+}]_i$ baselines were recorded. Local delivery of ACh was initiated by applying $V_{EB} = 4$ V to the IBJT. As cells located at the collector outlet were exposed to ACh, an immediate increase of the $[Ca^{2+}]_i$ was observed (Fig. 4*B*). ACh delivery was terminated by switching the IBJT to the off state, which resulted in a rapid decrease in local ACh concentration due to diffusion out into the cell media. As the $[Ca^{2+}]_i$ declined and returned to a lower level, cells were reexposed to ACh by applying $V_{EB} = 4$ V, and again, a Ca^{2+}-response was induced. In control experiments, when the procedure was repeated using NaCl (0.1 M) as emitter electrolyte, no intracellular Ca^{2+} response was observed, whereas a prompt response was initiated by manual addition of ACh to the cells.

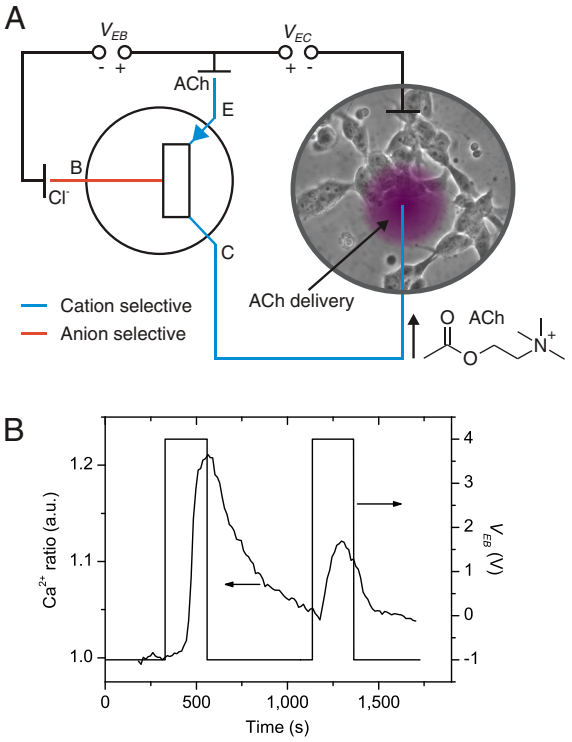

Fig. 4. The IBJT as an addressable delivery point for modulation of neuronal cell signaling. (*A*) Schematic illustration of the IBJT in a circuitry. SH-SY5Y cells were cultured on top of the collector electrode and ACh was placed on the emitter electrode. When switching on the device, ACh migrates through the E-C circuit and is released to the cells. (*B*) Intracellular Ca^{2+} recording of ACh stimulated SH-SY5Y cell. Switching V_{EB} on/off regulates ACh delivery, which then modulates the cellular Ca^{2+} response.

Based on this first proof-of-principle experiment of ACh delivery to cholinergic cells, the use of the IBJT can be expanded to include a vast number of positively charged biomolecules, acting on different cell receptors, to any type of cells or tissue in vitro. By connecting a large number of IBJTs in a chemical circuit, an addressable delivery matrix can be achieved, which provides a novel interface for biological systems. Generation of controlled, complex, high-resolution signaling patterns will be of utmost importance to increase our understanding in areas such as cell communication in neuronal networks.

Conclusions

Despite the fundamental differences between selective membranes and semiconductors, bipolar transistors based on these materials show strikingly many similarities. The current rectification analogy between bipolar membranes and semiconductor *pn*-junctions is well established. With this work, we extend the analogy to include transistors and we show how a solid-state ion bipolar junction transistor, the *pnp*-IBJT, can be constructed in a similar way as its *pnp*-semiconductor counterpart. In the next phase, we aim to construct the complementary version, i.e., the *npn*-IBJT, to modulate anion transport. This opens up the possibility for addressable delivery systems for both positively and negatively charged ions and biomolecules, as well as for complementary ion circuits. Whereas we have demonstrated the use of the IBJT in modulating neuronal cell signalling, we envisage that the IBJT will have major impact as the key component for amplification, addressing and processing of chemical signals in complex circuits for drug delivery (27), lab-on-a-chip (28), sensor (29), and electrochemical (30, 31) applications.

Materials and Methods

Manufacturing. The surface of PEDOT:PSS (AGFA-Gevaert Orgacon™ F-350), coated on a polyethylene terephthalate (PET) substrate, was cleaned using 1112A remover (Shipley), then rinsed in acetone and deionized water. Shipley 1805 photoresist was deposited onto the PEDOT:PSS surface after pretreatment with O_2-plasma and primer (hexamethyldisilazane). PEDOT:PSS was patterned using a O_2/CF_4 plasma etch-step. Overoxidized patterns of PEDOT:PSS were achieved by exposing the unsealed PEDOT:PSS areas to a sodium hypochlorite solution (1% (vol/vol), 50 s). A layer of SU-8 2010 (MicroChem) was patterned on top of the electrode configuration. A mixture of poly(ethylene glycol diacrylate) (M_n 575, Sigma) and 2% (w/w) 1-hydroxycyclohexyl phenyl ketone (Sigma) was placed in an opening in the SU-8 by differential wetting and photopolymerized (30 s, VL-208 BL 32 W, 365 nm) in N_2 atmosphere. An approximately 0.8×5 mm stripe of Fumatech FAB membrane was cut and laminated on to the device by heating from underneath (hotplate 110 °C, 5 s). The stack was sealed by a PDMS mixture (10:1 Sylgard 186) and cured at 80 °C for 1 h.

Characterization. Devices were soaked in deionized water for 24 h prior to use. Voltages were applied with a Keithley 2602 source meter controlled via LabVIEW (sample rate 5 Hz), and aqueous 0.1 M NaCl electrolytes were used throughout the characterization. All devices were repeatedly turned on and off, typically about five times, until stable performance was reached. Each type of characterization was repeated on different devices at least three times, representative recordings are presented.

Cell Cultivation. Human neuroblastoma SH-SY5Y cells (ATCC nr: CRL-2266) were propagated according to instructions from the supplier. At 80% confluency, cells were reseeded at a ratio of 1:5. One to two days prior to experiments, cells were seeded in fresh medium on the bovine fibronectin (5 $\mu g/cm^2$) (Sigma) precoated collector electrode, whereas water was placed on the emitter and base electrodes to allow hydration of the polymer.

Intracellular Ca^{2+} Recordings. Cells were loaded with the membrane-permeable Ca^{2+}-sensitive dye FURA-2 AM. ACh (80 μl, 10 mM in 0.1 M NaCl, Fluka) was applied as emitter electrolyte and NaCl (80 μl 0.1 M, Sigma) as base electrolyte. Cells were monitored using an upright Nikon Eclipse 80i with a 40 × /0.80 epifluorescence objective. Excitation at 340 and 380 nm was achieved with a DeltaRAM illuminator and a DeltaRAM-V monochromator with a computer controlled SC500 shutter controller. Emission (510 nm) was collected every 13 s with a Photometrics Coolsnap CCD camera. Data were analyzed using PTI ImageMaster3 Software. Each set of experiments was repeated a minimum of three times; one representative recording is presented.

ACKNOWLEDGMENTS. The authors acknowledge Professor Robert Forchheimer, Dr. Edwin Jager, and Dr. Daniel Simon, all at Linköping University, as well as Dr. Mats Sandberg at Acreo AB, for fruitful discussions. The research was financed by the Swedish Foundation for Strategic Research (OBOE Strategic Research Center for Organic Bioelectronics), the Knut and Alice Wallenberg Foundation, the Royal Swedish Academy of Science, and the Önnesjö Foundation.

1. Choi BD, Kwon OK (2004) Data and gate line sharing methods for low-cost and high-pixel density TFT-LCDs. *Electron Lett* 40(4):240–241.
2. Dodabalapur A, et al. (1998) Organic smart pixels. *Appl Phys Lett* 73(2):142–144.
3. Sze S (2002) *Semiconductor Devices: Physics and Technology* (John Wiley & Sons, New York), 2nd Ed.
4. Burgmayer P, Murray RW (1984) Ion gate electrodes—Polypyrrole as a switchable ion conductor membrane. *J Phys Chem* 88(12):2515–2521.
5. Karnik R, et al. (2005) Electrostatic control of ions and molecules in nanofluidic transistors. *Nano Lett* 5(5):943–948.
6. Kang MS, Martin CR (2001) Investigations of potential-dependent fluxes of ionic permeates in gold nanotubule membranes prepared via the template method. *Langmuir* 17(9):2753–2759.
7. Nishizawa M, Menon VP, Martin CR (1995) Metal nanotubule membranes with electrochemically switchable ion-transport selectivity. *Science* 268(5211):700–702.
8. Nam SW, Rooks MJ, Kim KB, Rossnagel SM (2009) Ionic field effect transistors with sub-10 nm multiple nanopores. *Nano Lett* 9(5):2044–2048.
9. Kontturi K, Murtomäki L, Manzanares JA (2008) *Ionic Transport Processes: In Electrochemistry and Membrane Science* (Oxford Univ Press, Oxford).
10. Mafe S, Ramirez P (1997) Electrochemical characterization of polymer ion-exchange bipolar membranes. *Acta Polym* 48(7):234–250.
11. Strathmann H, Krol JJ, Rapp HJ, Eigenberger G (1997) Limiting current density and water dissociation in bipolar membranes. *J Membr Sci* 125(1):123–142.
12. Chiang CK, et al. (1977) Electrical-conductivity in doped polyacetylene. *Phys Rev Lett* 39(17):1098–1101.
13. Roncali J (1992) Conjugated poly(thiophenes) - synthesis, functionalization, and applications. *Chem Rev* 92(4):711–738.
14. Heywang G, Jonas F (1992) Poly(alkylenedioxythiophene)s—New, very stable conducting polymers. *Adv Mater* 4(2):116–118.
15. Pei Q, Zuccarello G, Ahlskog M, Inganäs O (1994) Electrochromic and highly stable poly (3,4-ethylenedioxythiophene) switches between opaque blue-black and transparent sky blue. *Polymer* 35(7):1347–1351.
16. Tehrani P, et al. (2005) Patterning polythiophene films using electrochemical overoxidation. *Smart Mater Struct* 14(4):21–25.
17. Rubinstein I, Zaltzman B, Kedem O (1997) Electric fields in and around ion-exchange membranes. *J Membr Sci* 125(1):17–21.
18. Manzanares JA, Murphy WD, Mafe S, Reiss H (1993) Numerical-simulation of the nonequilibrium diffuse double-layer in ion-exchange membranes. *J Phys Chem* 97(32):8524–8530.
19. Zabolotskii VI, Manzanares JA, Mafe S, Nikonenko VV, Lebedev KA (2002) Steady-state ion transport through a three-layered membrane system: A mathematical model allowing for violation of the electroneutrality condition. *Russ J Electrochem* + 38(8):819–827.
20. Sokirko AV, Ramirez P, Manzanares JA, Mafe S (1993) Modeling of forward and reverse bias conditions in bipolar membranes. *Ber Bunsen-Ges Phys Chem Chem Phys* 97(8):1040–1049.
21. Cheng LJ, Guo LJ (2009) Ionic Current Rectification, Breakdown, and Switching in Heterogeneous Oxide Nanofluidic Devices. *ACS Nano* 3(3):575–584.
22. Xia YN, Whitesides GM (1998) Soft lithography. *Annu Rev Mater Sci* 28:153–184.
23. Isaksson J, et al. (2007) Electronic control of Ca^{2+} signalling in neuronal cells using an organic electronic ion pump. *Nat Mater* 6(9):673–679.
24. Simon DT, et al. (2009) Organic electronics for precise delivery of neurotransmitters to modulate mammalian sensory function. *Nat Mater* 8(9):742–746.
25. Tybrandt K, et al. (2009) Translating electronic currents to precise acetylcholine-induced neuronal signaling using an organic electrophoretic delivery device. *Adv Mater* 21(44):4442–4446.
26. Lukas RJ, Norman SA, Lucero L (1993) Characterization of nicotinic acetylcholine receptors expressed by cells of the sh-sy5y human neuroblastoma clonal line. *Mol Cell Neurosci* 4(1):1–12.
27. Abidian MR, Kim DH, Martin DC (2006) Conducting-polymer nanotubes for controlled drug release. *Adv Mater* 18(4):405–409.
28. Weigl BH, Bardell RL, Cabrera CR (2003) Lab-on-a-chip for drug development. *Adv Drug Delivery Rev* 55(3):349–377.
29. Mabeck JT, Malliaras GG (2006) Chemical and biological sensors based on organic thin-film transistors. *Anal Bioanal Chem* 384(2):343–353.
30. Nilsson D, et al. (2002) Bi-stable and dynamic current modulation in electrochemical organic transistors. *Adv Mater* 14(1):51–54.
31. Bernards DA, Malliaras GG (2007) Steady-state and transient behavior of organic electrochemical transistors. *Adv Funct Mater* 17(17):3538–3544.